Hindawi
Shock and Vibration
Volume 2023, Article ID 9107240, 24 pages
https://doi.org/10.1155/2023/9107240

Research Article

Experimental Study on Seismic Fatigue Capacity of High- and Mild-Strength Structural Steels with and without Corrosion

Mohammad Hossein Razmkhah, Mohsen Ghaderi, and Mohsen Gerami

Department of Civil Engineering Faculty, University of Semnan, Semnan, Iran

Correspondence should be addressed to Mohsen Gerami; mgerami@semnan.ac.ir

Received 2 August 2023; Revised 14 October 2023; Accepted 18 October 2023; Published 4 November 2023

Academic Editor: Junyan Yi

The test results on hourglass specimens of steel under repetitive sine loads provide graphs that indicate the stress range in terms of the number of cycles to failure and are known as S-N curves. Using this curve, it is determined that if the applied stress is less than a certain level, failure will not occur as the number of load cycles increases. The S-N curve can be affected by several factors such as yield stress, temperature, surface properties, and corrosion. In this research, the S-N curve has been investigated for two types of high-strength steels, S690 and S460, as well as two types of mild-strength steels, S235 and S355, at 25°C, and S355 with corrosion. The numbers of samples used for S235 and S460 steels were 45 each while S355 and S690 steels were 36 each and for S355 with corrosion was 15 with the high cycle fatigue curve obtained for them. To investigate the effect of plate thickness on the high cycle fatigue of the samples, four sets of 24-piece S235 steel samples, being 96 samples in total, were made of plates with different thicknesses of 8, 12, 15, and 20 mm and tested. Finally, a four-story three-span steel moment frame was designed, and under the Northridge earthquake record, the high cycle fatigue was investigated. It was observed that the high cycle fatigue was not effective for the mentioned structure under the Northridge earthquake record, but in the corroded structure, damage from high cycle fatigue occurs under this record.

1. Introduction

The term fatigue was first used by a French mathematician named Punklet in his book in French in 1841 [1]. In 1850, Wohler first systematically examined the fatigue behavior of steel [2]. Since the concept of metal fatigue was unknown at the time, the microscopic and mechanical aspects of the fatigue data were not well understood, and therefore, Wohler's aim was to obtain rail fatigue data for which the fatigue characteristics were not considered up to that time. Attempts for obtaining fatigue parameters for different materials have continued to this day since Wohler introduced railroad design for safe design [3]. Fatigue in microstructure scale is a complex process of formation and cracking which depends on microstructural features [4–9].

Ultralow cycle, low cycle, and high cycle fatigue are all types of fatigue [10]. In ultralow cycle fatigue, failure will be malleable due to strain greater than the yield stress in the structure, which is characterized by high plastic strain amplitudes (several plastic strains) and a very small number of load cycles (typically about 10–20 cycles) [11–14]. When a structure experiences low cycle fatigue, which has cycles between 10^2 and 10^4, the strain is less than the yield strain, causing brittle failure [15]. High cycle fatigue is characterized by a high number of cycles (more than 10^4 cycles) and, like low-cycle fatigue, a brittle failure with a strain less than the yield strain at the time of failure [16].

Considering alloy design, conditions that contribute to nucleation resistance and growth of microcracks under fatigue load may not help resist the growth of large macrocracks, and vice versa. For example, fine grain tends to resist more nucleation and microcracks growth, and in this case, the grain boundaries act as deflectors or stoppers of microcracks, thus reducing the growth rate of microcracks of fatigue. However, as the crack grows and the length of cracks increases, fine-grained flatter the crack path and elevate the crack growth rate. In contrast, coarse-grained materials tend to create a rougher crack path for macrocracks, and due to crack closure and the

crack tip deflection mechanism, the rougher the crack path, the greater the resistance to the growth of large cracks. As mentioned, many variables are involved in fatigue, so it is best to do the test to consider all of factors.

In the hot rolling process, the thickness of steel slabs diminishes by passing through two rollers, while the direction of the slab is opposite to the direction of rotating of the rollers, and if the width of the slab is constant, its length rises [17]. The general hot rolling process is displayed in Figure 1.

The processes involved in hot rolling are as follows:

Reheating: the slab is heated to a temperature of 1200–1250°C in a furnace to remove dendrites from casting as well as to combine most of the alloying elements.

Rough rolling: before rolling, the scale created during the heating stage is removed by spraying high-pressure water in the descaling box. The slab then moves to the roughing mill. At this step, the thickness of the slab is reduced between 270 mm and 50 mm by passing through the roller. Also, its width is altered using vertical rollers installed on the sides. After shaping, it is transferred to the next stage using the transfer table.

Finish rolling: the final forming stage consists of five to seven rollers. The slab enters this part, with temperature and thickness measured by sensors for the final mill at this stage and the temperature adjusted using the speed of the rollers.

Cooling: after rolling, the strip is cooled by a water flow.

Coiling: in the last step, the strip temperature is measured and the strip is coiled by the coiler.

Due to the difference in the cooling rate of the sample, for example, in the cooling stage, the size of the grain changes with the thickness of the steel, and near the surface, the steel grain will have a finer structure than the center of the strip because it cools faster (the surface of the metal cools quickly, and the crystals on the surface do not get a chance to grow, but in the center of the section, due to the fact that the cooling speed is lower than the surface, the crystals can grow). As mentioned, the finer the steel grain, the slower the crack nucleation rate, but the higher the crack growth rate, and if the grain is coarse, the higher the crack nucleation rate but the slower the growth rate.

The estimated annual cost of corrosion in the United States of America is about 30 billion dollars, which shows a huge economic loss. Wherever there is metal, corrosion occurs with different degrees and intensities. When protective coatings and cathodic protection systems are either absent or ineffective, steel structures exposed to harsh environments such as urban, industrial, and marine environments, such as transmission towers, steel bridges, industrial buildings, and offshore platforms, show signs of surface corrosion [18, 19].

Significant degradation in the strength and ductility of corroded steel plates, as well as a large decrease in the energy dissipation capability of corroded H-shaped steel columns with an increase in the percentage of corrosion, were observed using the tensile test [20, 21].

Corroded steel members are more likely to experience damage and failure when a strong earthquake occurs, for example, the Wen Chuan earthquake in China, the Osaka earthquake in Japan [22], the Northridge earthquake in 1994 [23], and the Alaska earthquake in 1964, where corroded structures experienced more damage and failure than other structures.

To study cyclic fatigue in this paper, S-N curves are used, in which the vertical axis is the stress applied to the structure (σ) and the horizontal axis is the number of cycles that can be tolerated by the structure at the stress applied to the structure. In order for the structure not to be damaged under high cycle fatigue, the amount of stress applied in each cycle should be lower than the corresponding amount of stress that cycle which is obtained from the S-N diagram for the desired material.

Unfortunately, a one S-N diagram cannot be used for all metals, and each metal has its own S-N curve, which changes under factors such as corrosion, surface finishing, and treatments. [24], where S-N diagram requires a large number of tests at different stress intensities and a large number of cycles, which requires considerable time to perform the test. In this study, the Wohler method was used to perform the cyclic fatigue test. In the Wohler method, or the same method of the four-point bending test, which is very common, one half of the sample is under tensile stress at all times, while the other half, which is symmetrical to the first half, is under compressive stress, and thus, in a complete cycle, the average received stress (Sm) is zero (see Figure 2). The mean stress, Sm, can have a substantial influence on fatigue behavior. In general, tensile mean stresses are detrimental, and compressive mean stresses are beneficial. Substantial investigation of tensile mean stress influence on long-life fatigue strength has been made [24].

s_a is equal to the applied stress and also R is equal to -1 called the "fully reversed" condition, and the loading frequency is 120 Hz selected. Mean, Sm, maximum, $s_{\max}$, minimum, $s_{\min}$, and range, ΔS, of applied stress are shown in the following equations and also are displayed in Figure 3.

$$S_a = \frac{\Delta S}{2} = \frac{S_{\max} - S_{\min}}{2}, \tag{1}$$

$$S_m = \frac{S_{\max} + S_{\min}}{2}, \tag{2}$$

$$R = \frac{S_{\min}}{S_{\max}}. \tag{3}$$

The samples to be tested for cyclic fatigue must have polished surfaces so that the surface roughness of the samples does not interfere with the results. Figure 4 displays the details of fatigue sample as well as a number of samples before and after failure. To report the amount of applied stress, the stress range s or the stress amplitude $S_a = S/2$ is used. In this research, all applied stresses are in the form of S_a.

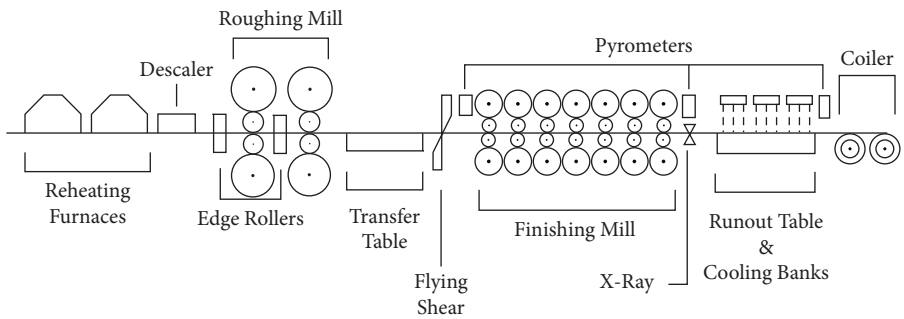

Figure 1: The hot rolling process [17].

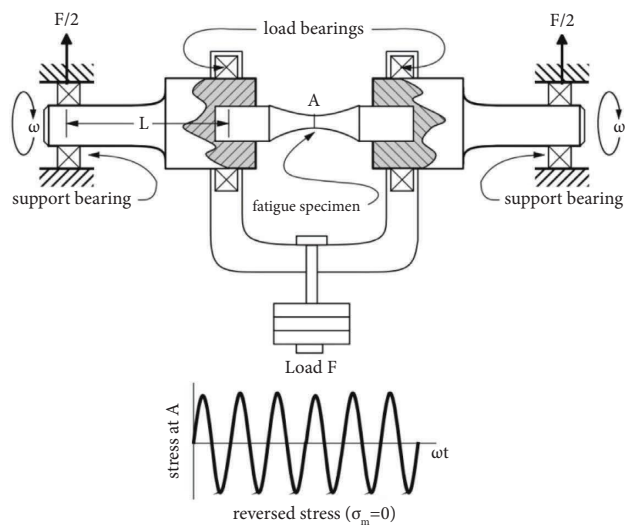

Figure 2: Rotating bending fatigue testing machine [24].

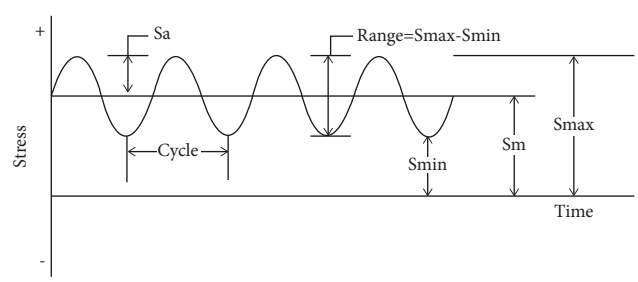

Figure 3: Nomenclature for constant amplitude cyclic loading [24].

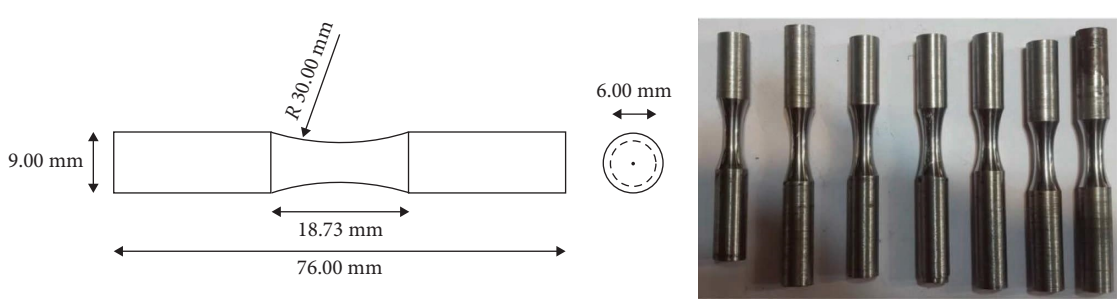

(a) (b)

Figure 4: Continued.

(c)

Figure 4: (a) Sample detail for the fatigue test [25], (b) samples before the high cycle fatigue test, and (c) broken specimens after the high cycle fatigue test.

Another parameter that affects the S-N curve is corrosion. In the following, explanations are given regarding the classification of corrosive environments and the amount of consumption for different years.

This research investigates high cycle fatigue in common steels in civil engineering, which include high-strength steels (S690 and S460) and mild-strength steels (S235 and S355) used in the construction industry, and also investigates the effect of thickness on the fatigue limit. Since steel is prone to corrosion in environments and atmospheric corrosion is one of the most common types of corrosion in steel structures, at the end of this research, the effect of corrosion on the fatigue of steel structures is investigated. The process of research is shown in Figure 5.

In the following, explanations are given regarding the classification of corrosive environments and the amount of consumption for different years.

2. Corrosion

Corrosion is defined as the destruction or corruption of a material as a result of reaction with the environment in which it is located. Some authorities insist that corrosion is limited to metals, but in a comprehensive classification, even nonmetallic materials such as plastic and ceramics are destroyed and corroded in the vicinity of chemicals and even sunlight [26].

If the environments that cause corrosion are divided, they can be divided into three general areas: corrosion in the atmospheric environment, corrosion in seawater, and corrosion in soil. In this research, atmospheric corrosion has been investigated. Atmospheric corrosion is mainly due to moisture and oxygen, but the problem becomes more critical with impurities such as sulfur compounds and sodium chloride.

The ISO 9223 standard examines the corrosion rate in the first year in different atmospheric environments. This standard divides atmospheric corrosive environments into 6 categories, which are shown in Table 1.

By using the ISO 9224 standard, which is an annex to the ISO 9223 standard, the amount of corrosion can be obtained for different years based on the category of the corrosive environment (Table 2).

The corrosion rate considered for this article corresponds to 20 years of corrosion in a corrosive environment with the CX category, which is related to the subtropical region with high humidity and high SO_2 pollution (SO_2 more than 250 mg/m^3).

3. The Method of Creating Corrosion

It is clear that it can in some way create the corrosion that occurs in natural conditions in the samples with the necessary instructions, with the difference that the time when the corrosion occurs in the samples should be much shorter than the time when the corrosion occurs in the real area, and it should be able to be implemented with the same accuracy. ASTM G60-1 standard is used to simulate corrosion; this standard specifies the conditions of simulation corrosion for atmospheric conditions [29].

The specimens should be humidity cycle three times per day, as shown in Figure 6, and a dip cycle once a day.

The temperature of the air in the test chamber is 52 ± 1°C. The range of relative humidity can be extended by adding a drying period to the humidity cycle. The minimum relative humidity shall be ≤20%, and the maximum relative humidity shall be ≥95% for each cycle.

The dip solution should be prepared by dissolving 1% sodium chloride (NaCl), 1% calcium chloride ($CaCl_2$), and 0.1% sulfuric acid (H_2SO_4) by solution weight in water (See Figure 7). The solution volume to specimen surface area ratio should be a minimum of 250 mL/cm^2.

One dip cycle shall consist of three 5 min immersion periods. The dip solution is drained from the test chamber for a 1 min period between each immersion period. The samples before corrosion and after 5 months of exposure in the corrosion simulator environment can be seen in Figures 8(a) and 8(c). The two ends of the sample, which are placed in the clamp of the fatigue testing machine, are coated with epoxy to prevent the corrosion of these two areas.

The amount of corrosion in the samples is equal to 10%. For a column with S355 material with a total depth of 400, a flange width of 250, a flange thickness of 20, and a web thickness of 10 mm, the amount of corrosion corresponding to 20 years in environmental conditions CX (see Table 1), which is the weather conditions in an industrial area, is equal to 10%.

The choice of 20 years when the structure is exposed to a corrosion environment is because the protective coating of the structures to prevent corrosion usually disappears after 5 years, and after the end of this time, the main structure undergoes corrosion [30]. Considering that the life of a structure is assessed to be 30 years, an estimate of the

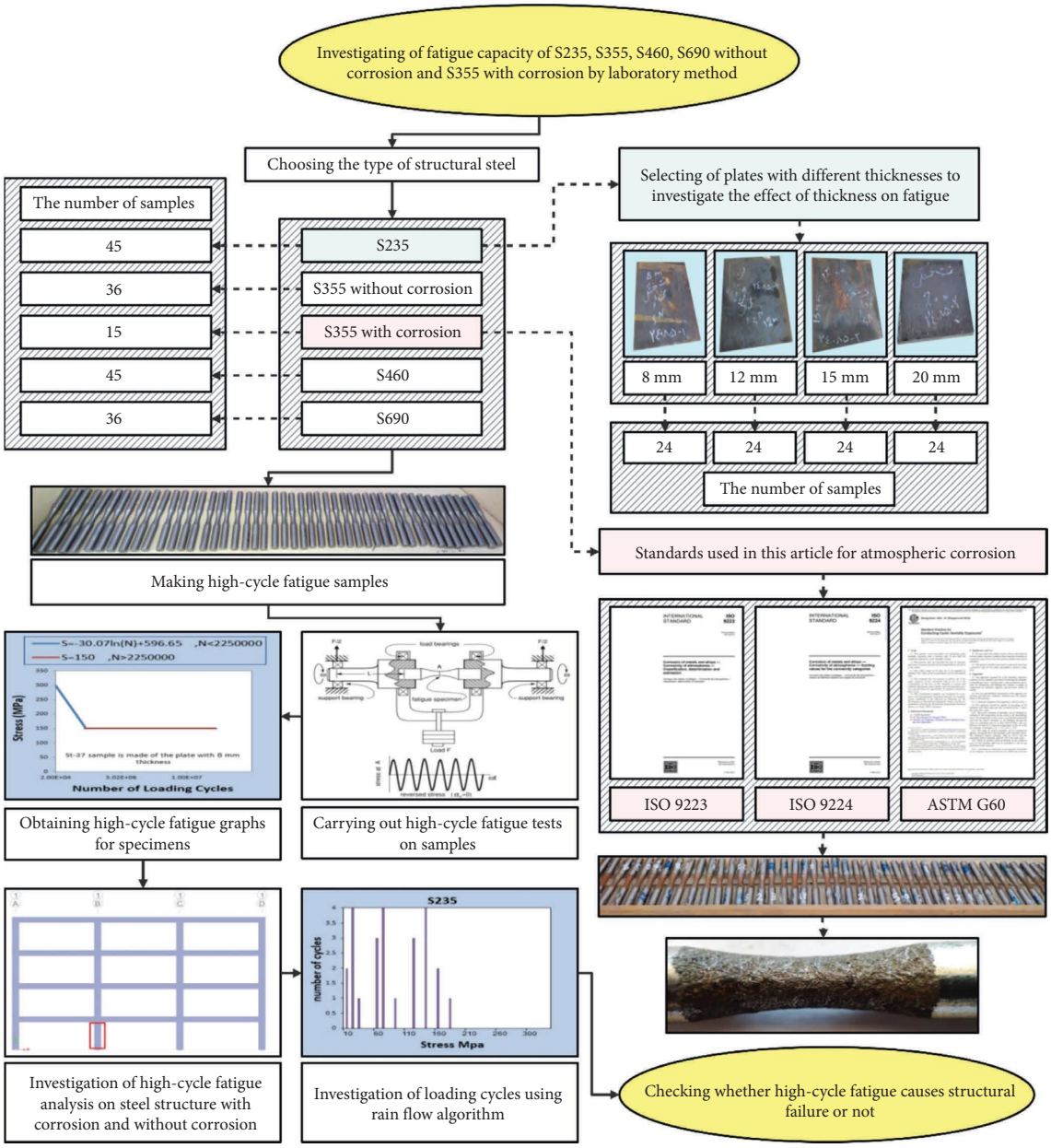

Figure 5: Flowchart of the research process.

capacity of a structure that undergoes corrosion, during this period and still has 5 years of its life remaining, is necessary.

4. Stress-Strain Diagrams of S235, S355, S460, and S690 Steels

The chemical composition of S235, S355, S460, and S690 steels is given in Table 3. The strain-stress diagram of the steels used in this study to test the high cyclic fatigue is shown in Figure 9. It can be seen that as the strength of the steel rises, its ductility decreases. For example, the ultimate strength of S690 steel is one and a half times that of S235 steel, but its ductility is 0.3 times that of S235 steel.

5. Sensitivity of S-N Diagram to Plate Thickness

According to the thickness of the plates produced in hot rolling mills in Iran, to investigate the effect of plate thickness in high cycle fatigue, four plates with thicknesses of 8, 12, 15, and 20 mm were selected and from each plate, 24 hourglass samples have been made for high cycle fatigue testing (see Figure 10).

Table 1: Classification of atmospheric corrosive environments based on ISO 9223 [27].

Corrosivity category	Corrosivity	Typical environments—examples	
		Indoor	Outdoor
C1	Very low	Heated spaces with low humidity and insignificant pollution, e.g., offices, schools, museums	Dry or cold zone, atmospheric environment with very low pollution and time of wetness, e.g., certain deserts, Central Arctic/Antarctica
C2	Low	Unheated spaces with varying temperature and relative humidity. Low frequency of condensation and low pollution, e.g., storage, sport halls	Temperate zone, atmospheric environment with low pollution ($SO_2 < 5\,mg/m^3$), e.g., rural areas, small towns Dry or cold zone, atmospheric environment with short time of wetness, e.g., deserts, subarctic areas
C3	Medium	Spaces with moderate frequency of condensation and moderate pollution from the production process, e.g., food-processing plants, laundries, breweries, and dairies	Temperate zone, atmospheric environment with low pollution (SO_2: $5\,mg/m^3$ to $30\,mg/m^3$) or some effects of chlorides, e.g., urban area and coastal area with low deposition of chlorides Subtropical and tropical zone, atmosphere with low pollution
C4	High	Spaces with high frequency of condensation and high pollution from production processing plants, swimming pools	Temperate zone, atmospheric environment with low pollution (SO_2: $30\,mg/m^3$ to $90\,mg/m^3$) or substantial effect of chlorides, e.g., polluted urban area, industrial areas, and costal area without spray of salt water or exposure to strong effect of de-icing salts Subtropical and tropical zone, atmosphere with medium pollution
C5	Very high	Spaces with very high frequency of condensation and/or with high pollution from production process, e.g., mines, caverns for industrial purposes, unventilated sheds in subtropical and tropical zones	Temperate and subtropical zone, atmospheric environment with very high pollution (SO_2: $90\,mg/m^3$ to $250\,mg/m^3$) and/or significant effect of chlorides, e.g., industrial area, costal area, and sheltered positions on coastline
CX	Extreme	Spaces with almost permanent condensation or extensive humidity effects and/or with high pollution from the production process, e.g., unventilated sheds in humid tropical zones with penetration of outdoor pollution including airborne chlorides and corrosion-simulating particulate matter	Subtropical and tropical zones (very high time of wetness), atmospheric environment with very high SO_2 pollution (higher than $250\,mg/m^3$) including accompanying and production factors and/or strong effect of chlorides, e.g., extreme industrial areas, costal areas, and offshore areas, occasional contact with salt spray

Table 2: The amount of corrosion for different atmospheric environmental conditions in micrometers based on the ISO 9224 standard [28].

Metal	Corrosivity category	Exposure time years					
		1	2	5	10	15	20
Carbon steel	C1	1.3	1.9	3	4.3	5.4	6.2
	C2	25	36	58	83	103	120
	C3	50	72	116	167	206	240
	C4	80	115	186	267	330	383
	C5	200	287	464	667	824	958
	CX	700	1006	1624	2334	2885	3354

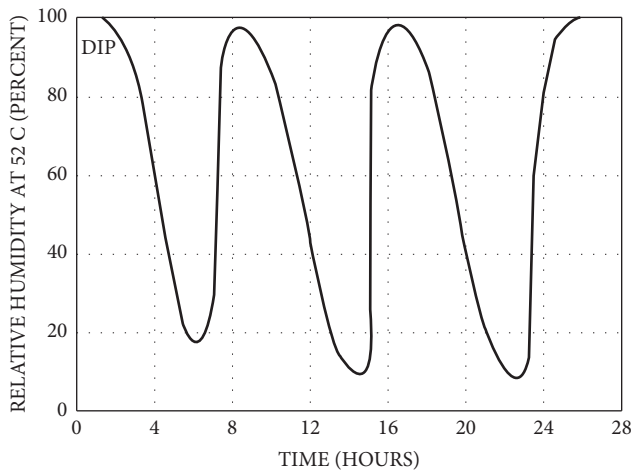

Figure 6: Humidity cycle (schematic) [29].

(a) (b) (c)

Figure 7: Materials for making corrosion solution: (a) sulfuric acid (H_2SO_4); (b) calcium chloride ($CaCl_2$); (c) sodium chloride (NaCl) [29].

The samples are placed in a rotating bending fatigue testing machine. The shape of the rotating bending fatigue testing machine used in this research is depicted in Figure 11.

The results of the high cycle fatigue test for the S235 sample made from different palates are reported in Table 4. Note that in this table, the results of each sample are the average of the results of the three samples at the same level of stress.

If the applied stress is plotted against the corresponding number of cycles, the S-N diagram of the selected steel is obtained. In this figure, a horizontal line is marked in red with a dashed line which indicates the fatigue limit (see Figure 12).

Because of the flattening of the S-N curve and the independence of fatigue life from stress cycles, this region is fatigue limit and is the region of infinite life, at least for ferrous alloys and titanium. A load can be applied indefinitely many times below this limit without experiencing failure.

Five different results are likely to be obtained from the same traction or fatigue test if five specimens of the same material, size, and surface finish are used. Ten different results are probably to be expected if there were ten test pieces. Increasing the number of specimens will not change this general outcome but will probably yield some new lower

Figure 8: (a) High cycle fatigue samples without corrosion inside the corrosion simulator environment. (b) High cycle fatigue samples after 5 months of exposure to a corrosive simulation environment. (c) The corroded surface in the middle part of the high cyclic fatigue specimen.

Table 3: The chemical composition of S235, S355, S460, and S690.

Steel grade	Chemical composition															
	C	Si	Mn	P	S	N	B	Cr	Cu	Mo	Nb	Ni	Ti	V	Zr	Al
S235	0.17	—	1.40	0.035	0.035	0.012	—	—	0.55	—	—	—	—	—	—	—
S355	0.20	0.55	1.60	0.035	0.035	0.012	—	—	0.55	—	—	—	—	—	—	—
S460	0.18	0.65	1.80	0.035	0.03	0.027	—	0.35	0.60	0.23	0.06	0.85	0.06	0.14	—	0.015
S690	0.20	0.80	1.70	0.025	0.015	0.015	0.005	1.50	0.50	0.70	0.06	2.00	0.05	0.12	0.15	0.015

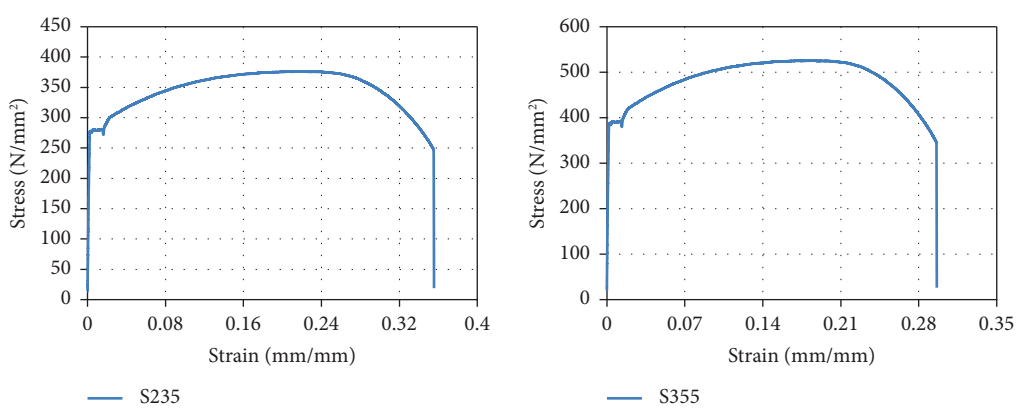

Figure 9: Continued.

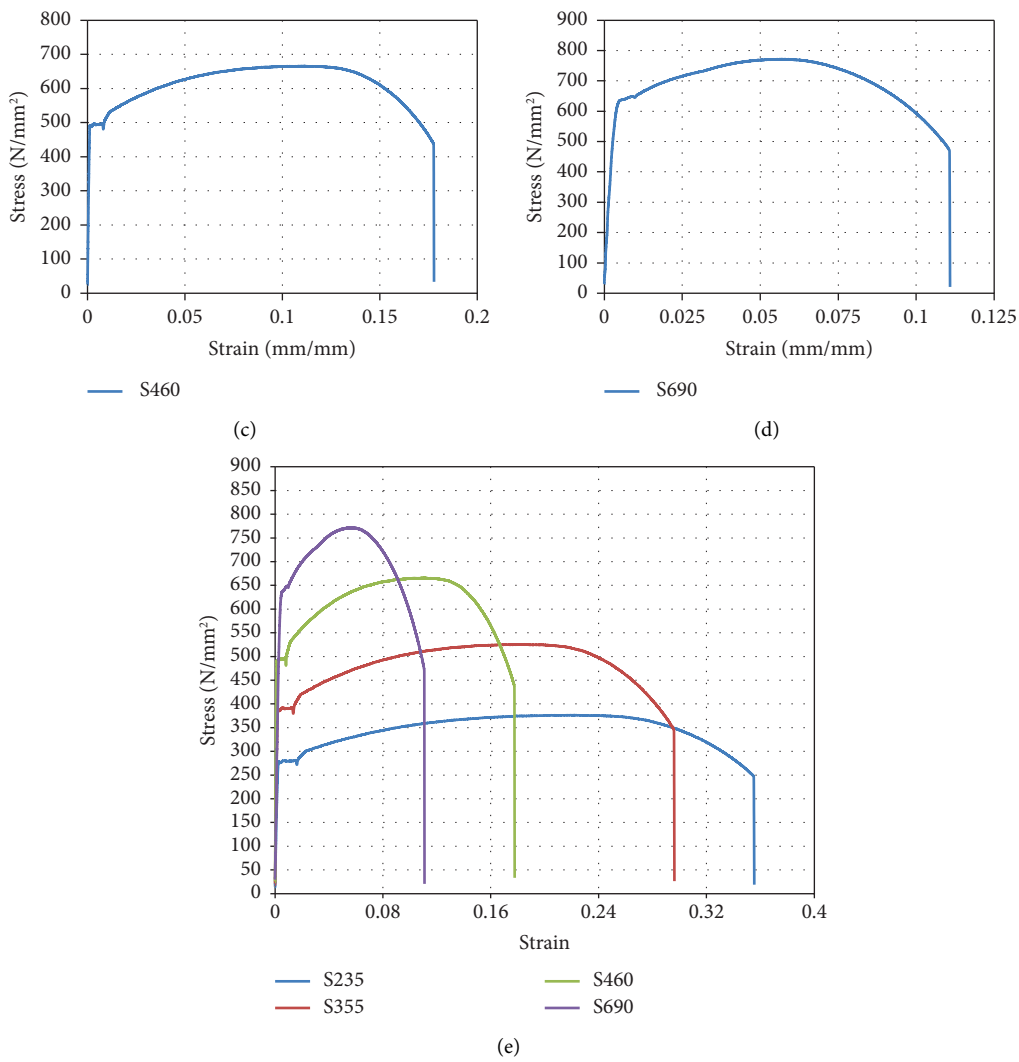

Figure 9: Stress-strain diagram of (a) S235, (b) S355, (c) S460, (d) S690 steels, and (e) all in one diagram.

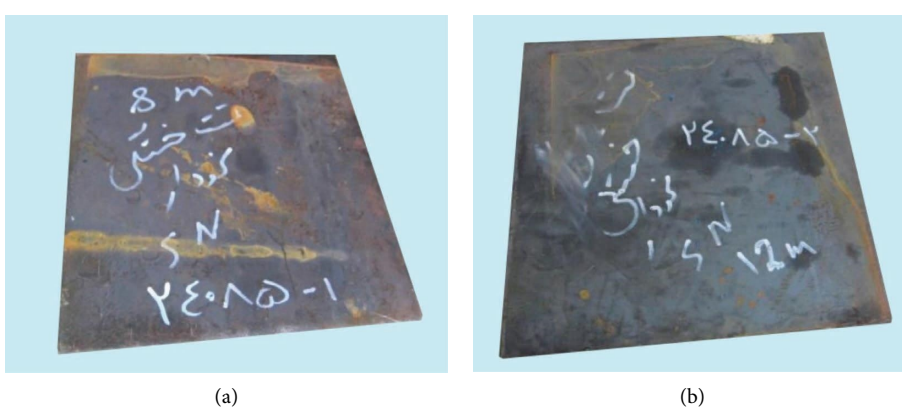

(a) (b)

Figure 10: Continued.

(c) (d)

Figure 10: Plates produced with different thicknesses of S235, (a) plates with thickness 8 mm, (b) plates with thickness 12 mm, (c) plates with thickness 15 mm, and (d) plates with thickness 20 mm.

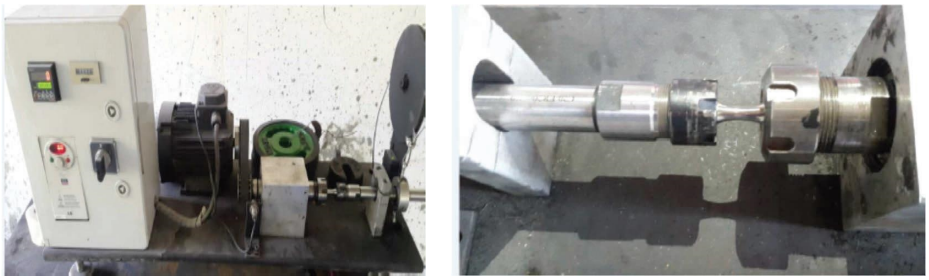

(a) (b)

Figure 11: Test process to obtain the S-N diagram: (a) rotating bending fatigue testing machine and (b) sample put in the fatigue testing machine.

Table 4: Results of the S235 high cycle fatigue test for thicknesses: (a) 8 mm, (b) 12 mm, (c) 15 mm, and (d) 20 mm.

Sample number	Stress applied (MPa)	Average number of cycles	Sample status at the end of the cycle
(a) Chemical properties of tde sample made of plate witd a tdickness of 8 mm			
Sample yield stress: 366 MPa		Sample ultimate stress: 510 MPa	
Mechanical properties of tde sample made of plate witd a tdickness of 8 mm			
1	290	19,524	Failure
2	250	198,364	Failure
3	220	325,655	Failure
4	180	725,365	Failure
5	160	1,852,745	Failure
6	155	2,251,122	Failure
7	150	12,525,951	No failure
8	148	12,875,210	No failure
(b) Chemical properties of tde sample made of plate witd a tdickness of 12 mm			
Sample yield stress: 320 MPa		Sample ultimate stress: 468 MPa	
Mechanical properties of tde sample made of plate witd a tdickness of 12 mm			
1	260	35,852	Failure
2	250	431,251	Failure
3	230	752,328	Failure
4	170	1,335,586	Failure
5	155	2,582,457	Failure
6	150	4,745,362	Failure
7	145	11,784,965	No failure
8	143	11,994,264	No failure

Table 4: Continued.

Sample number	Stress applied (MPa)	Average number of cycles	Sample status at the end of the cycle
(c) Chemical properties of tde sample made of plate witd a tdickness of 15 mm			
Sample yield stress: 352 MPa		Sample ultimate stress: 458 MPa	
Mechanical properties of tde sample made of plate witd a tdickness of 15 mm			
1	250	52321	Failure
2	235	325674	Failure
3	200	825432	Failure
4	180	998365	Failure
5	150	1665258	Failure
6	140	3259745	Failure
7	135	11258456	No failure
8	133	11856789	No failure
(d) Chemical properties of tde sample made of plate witd a tdickness of 20 mm			
Sample yield stress: 287 MPa		Sample ultimate stress: 467 MPa	
Mechanical properties of tde sample made of plate witd a tdickness of 20 mm			
1	230	86,325	Failure
2	200	165,250	Failure
3	180	428,693	Failure
4	160	825,784	Failure
5	140	1,746,325	Failure
6	120	2,325,458	Failure
7	115	12,582,865	No failure
8	113	12,985,147	No failure

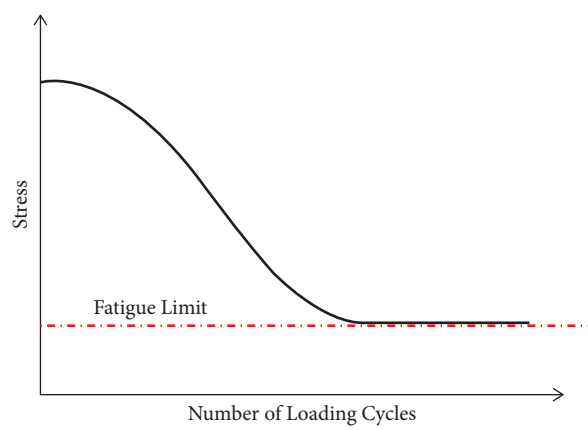

Figure 12: S-N diagram with a line indicating fatigue limit.

or higher value, as well [24]. In this research, the average of three data at each stress level is used to draw the S-N diagram.

Fatigue limit is the stress that, if the applied stress is equal to or less than it, the fatigue failure will never occur in the material, regardless of the number of loading cycles. As a result, in various industries such as aerospace engineering and civil engineering, for the design of structures, design based on the fatigue limit obtained from the S-N curve in such a way that the size of the section and the amount of stress applied to the member, always below the fatigue stress limit and in this way, the long life of the member is guaranteed.

Thus, in designing for parts where access is not possible to replace the part or the replacement cost is high, it is tried to observe the fatigue limit for that member so that the member does not get influenced by failure due to high cycle fatigue.

The S-N diagram of S235 sample made from plates with thicknesses 8, 12, 15, and 20 mm is shown in Figure 13.

As displayed in Figure 13, for samples made of steel plate with thicknesses of 8, 12, 15, and 20 mm, respectively, at stresses of 150 MPa, 145 MPa, 135 MPa, and 115 MPa, they become insensitive to cycle loads. The diagram can be divided into two parts according to Figure 14: one part of the

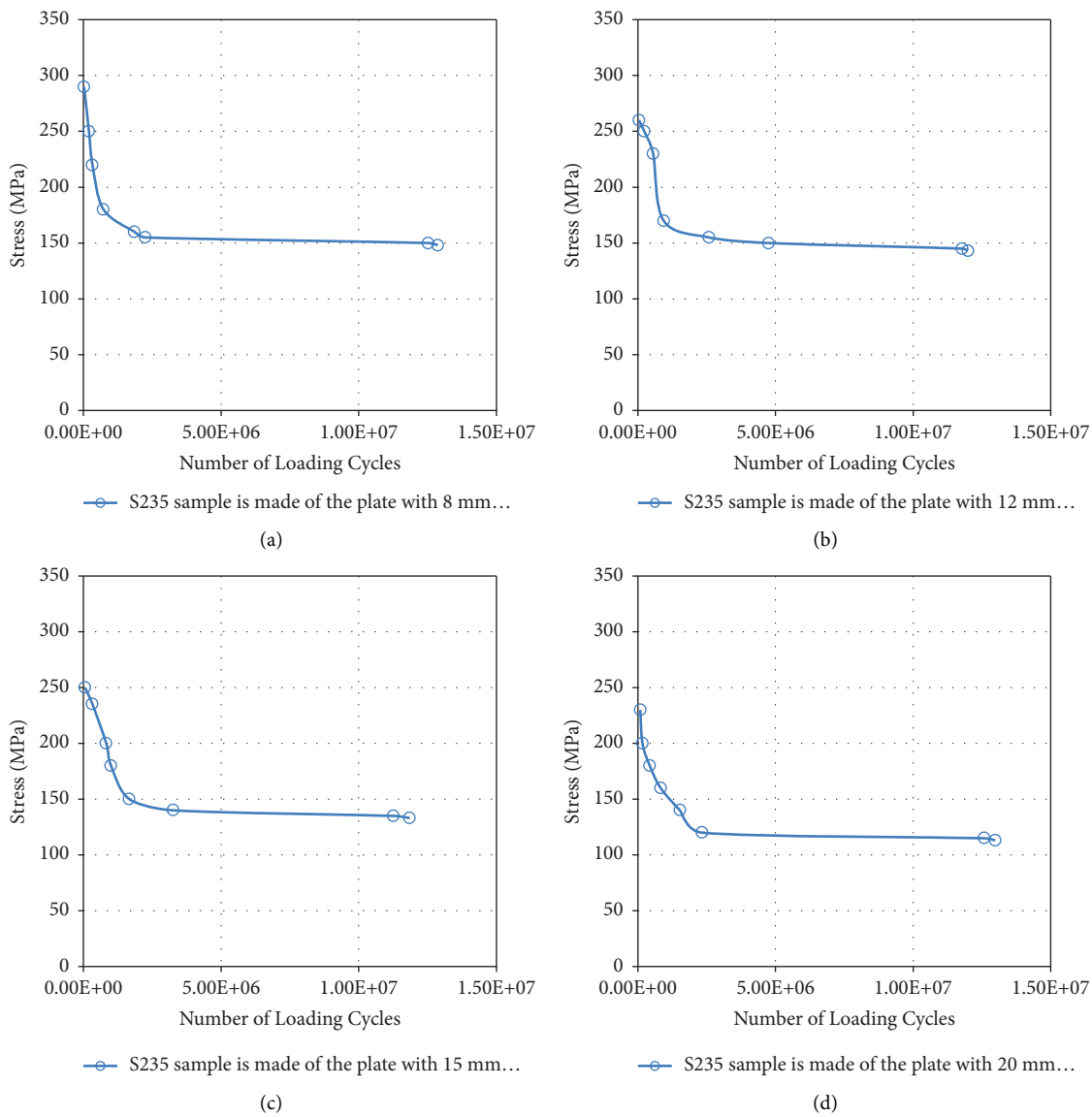

Figure 13: S-N diagram for S235 samples made of steel plate with thicknesses: (a) 8, (b) 12, (c) 15, and (d) 20 mm.

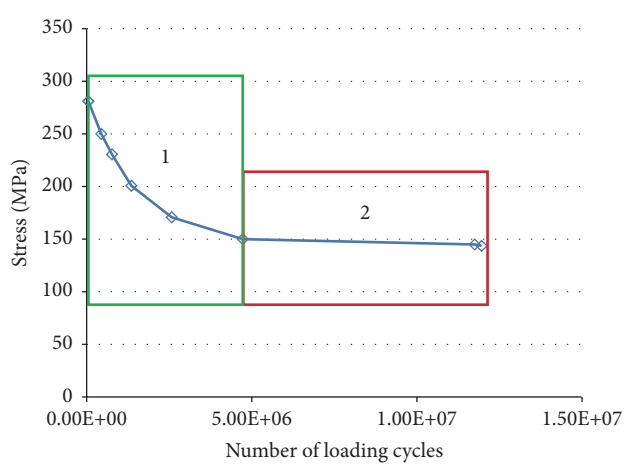

Figure 14: Dividing the S-N diagram into two parts sensitive to applied stress changes and insensitive.

diagram that changes with changing stress (area 1) and the other part that is not sensitive to stress change (area 2).

Fitted diagram S235 sample made from plates with thicknesses of 8, 12, 15, and 20 mm is presented in Figure 15. At the top of each diagram, the equation of the fitted lines corresponding to the different parts of the diagram is written. The correlation coefficient for fitted diagram S235 from plates with thicknesses of 8, 12, 15, and 20 mm is, respectively, equal to 0.98, 0.92, 0.94, and 0.99.

To evaluate the sensitivity of the S-N diagram to the thickness of the selected plate for producing the sample, the first part of the diagram for different thicknesses is drawn in Figure 16 and the second part of the diagram, which reveals the fatigue limit, is drawn in Figure 17. Observing Figure 16, it is concluded that if the sample made from plate with 8 mm thickness is considered as a basis, the maximum diagram changes in the first region compared to increasing the plate thickness to 20 mm are equal to 25%, suggesting that the fatigue strength of the sample made from plate with 20 mm thickness is about 25% less than the plate with 8 mm thickness.

For the second region of the S-N diagram (see Figure 17), the fatigue limit for S235 samples made of steel plate with a thickness of 20 mm is about 24% lower than the fatigue limit ratio of the sample made of steel plate with a thickness of 8 mm. The reason for this difference, as stated, is due to the different cooling rates in plates with different thicknesses in the production process and the size effect strongly depends on the average number of defects and inclusions in the material, which increases with thickness [24].

It can be seen that the size of the diameter is affecting the S-N curve of the material. A size factor C_{sz} that reduces the fatigue limit of the material as the specimen diameter increases. One of the most common and rather conservative formulas is that proposed by Shigley and Mitchell (equation (4)) [31].

$$C_{SZ} = \begin{cases} 1.0, & \text{if} \quad d \leq 8\,\text{mm}, \\ 1.189 \cdot d^{-0.097}, & \text{if} \quad 8 \leq d \leq 250\,\text{mm}, \end{cases} \tag{4}$$

where d is the diameter of the specimen or component. Being empirical in nature, equation (4) can be used only in the range of diameters considered, i.e., 8–250 mm.

If the sample with a diameter of 8 mm is set as a reference, according to equation (4), the fatigue limits 140, 137, and 133 are obtained for samples with a diameter of 12, 15, and 20 mm, respectively.

Another formula for fatigue limit for specimens with different diameters is proposed by Weibull (equation (5)) [24]. In this formula, l is the length of the specimen.

$$\frac{1}{C_{sz}} = \left[\frac{l_2}{l_1} \cdot \frac{(2 \cdot d_2 - 1)}{(2 \cdot d_1 - 1)}\right]^{1/m}. \tag{5}$$

If the sample with a diameter of 8 mm is set as a reference and the factor m is taken for steel 25, according to equation (5), the fatigue limits 147, 146, and 144 are obtained for samples with a diameter of 12, 15, and 20 mm, respectively. Table 5 shows the experimental values and the corresponding values obtained from equations (4) and (5)

Equation (6) was proposed by the authors for size factor in the fatigue limit for S235 specimens made of different plate thicknesses. The correlation coefficient for this equation is 0.97 and to use this formula, the fatigue limit must be in MPa.

$$C_{SZ} = \begin{cases} 1.0, & \text{if} \quad d \leq 8\,\text{mm}, \\ -0.027 \cdot d + 1.3, & \text{if} \quad 8 \leq d \leq 20\,\text{mm}. \end{cases} \tag{6}$$

6. High Cycle Fatigue Diagram of S235, S355, S460, and S690 Steels

The following are the fatigue diagrams for S235, S355, S460, and S690 steels, each containing 36, 45, 36, and 45 samples made of plates with a thickness of 10 mm, respectively. Table 6 lists the data related to the S235 steel high cycle fatigue test and Figure 18 depicts the diagram as well as the line fitted for it. The correlation coefficient for fitted diagram for the sample S235 is equal to 0.99.

The data for the S355 high cycle fatigue test are shown in Table 7 as well as the line fitted for its fatigue diagram in Figure 19. The correlation coefficient for fitted diagram for the sample S355 is equal to 0.99.

Table 8 relates to the high cycle fatigue test data of S460 steel and a fitted line is also drawn for it in Figure 20. The correlation coefficient for fitted diagram for the sample S460 is equal to 0.99.

Table 9 reports the data for the S690 high cycle fatigue test, as shown in Figure 21, as well as the line fitted for it. The correlation coefficient for fitted diagram S690 is equal to 0.99.

7. High Cycle Fatigue Diagram of S355 with Corrosion

S355 samples after being placed in the corrosion simulator with the process explained in Section 3 to simulate atmospheric corrosion with a corrosion rate of 10% (it should be mentioned that it took five months to create this amount of corrosion with the described process for the creation of corrosion), were subjected to the high cycle fatigue test, and the S-N diagram for it is shown in Figure 22(a). The S-N diagram of S355 with 10% corrosion and without corrosion is shown in Figure 22(b). As can be seen in Figure 22(b), the fatigue limit in the case of the sample with corrosion has decreased by 39%. In the area before the fatigue limit, the stress reduction is equal to 25%.

The reason for reducing the fatigue limit is explained below. Corrosion created using the ASTM G60-1 standard cause's uniform corrosion on the surface of the member, but due to the presence of materials such as calcium chloride and sodium chloride in solution, along with uniform corrosion, it causes pits on the surface of the member (Figure 23). These pits are caused by the concentration of stress in the member, and if the amount of stress concentration in the same area increases due to the singularity of stress in different cycles, it causes cracks to spread and causes the overall failure of the member.

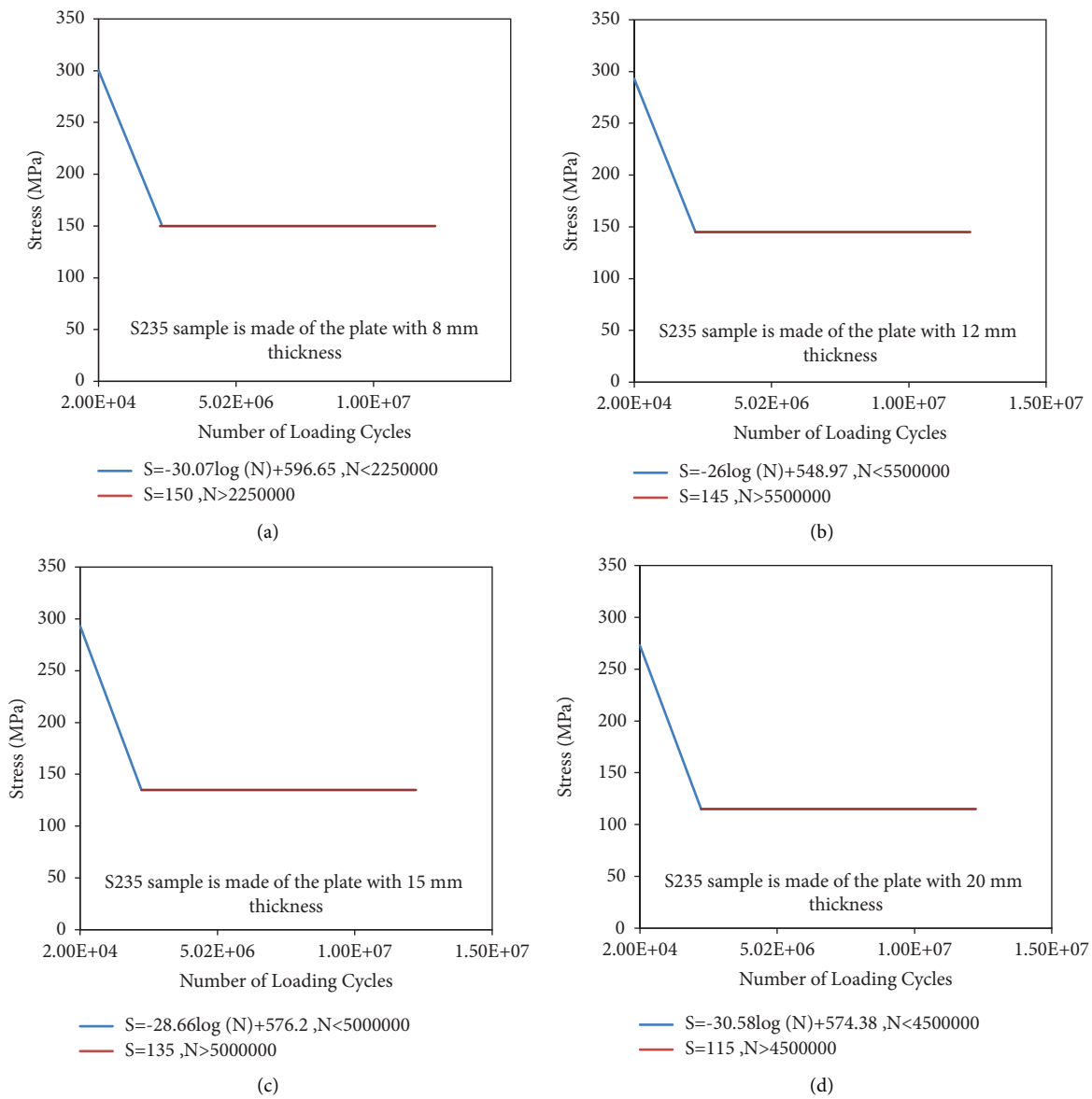

Figure 15: Fitted diagram of S235 samples made of steel plate with thicknesses: (a) 8, (b) 12, (c) 15, and (d) 20 mm.

8. Modeled Steel Moment Frame to Check High Cycle Fatigue

As stated in the Introduction section, there are three types of fatigue include ultralow cycle, low cycle, and high cycle. Ultralow cycle fatigue is strain-dependent, but in the case of high cycle and low cycle fatigue, it is stress-dependent. When a strong earthquake occurs, in such a way that the structure enters the nonlinear domain under the effect of this earthquake and the amount of strains in the structure exceeds the elastic strain limit, ultralow cycle fatigue becomes important. If the structure under earthquake record does not enter the nonlinear domain, high cycle and low cycle fatigue become important.

The important point is that this low-intensity earthquake that does not enter the whole structure into the nonlinear domain may happen many times in a certain period, which can be mentioned as an example; the Wenchuan earthquake occurred on May 12, 2008, by September 8, 2008, and there had been 42,719 total earthquakes [32].

Or as mentioned in the Introduction section, the Northridge earthquake in 1994, and the Alaska earthquake in 1964 where corroded structures experienced more damage and failure than other structures [23].

To investigate the high cyclic fatigue, a four-story three-span steel moment frame with a story height of 3 meters and a span length of 6 meters, as well as a load span of 6 meters perpendicular to the frame beams, according to ASCE/SEI 7–22 and AISC 360–22 for dead load 750 and live loads 200 kg/m^2 and soil type II design and is shown in Figure 24. The Northridge earthquake record of Canyon

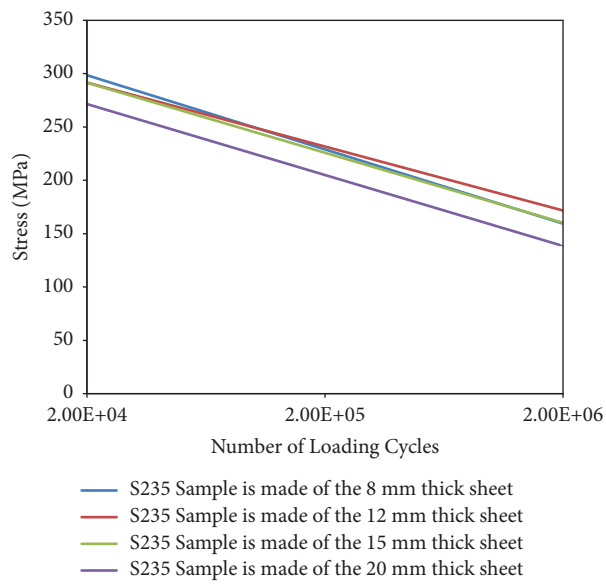

Figure 16: Fitted diagram of the first area of the S-N curve for S235 specimens made of plate with thicknesses of 8, 12, 15, and 20 mm.

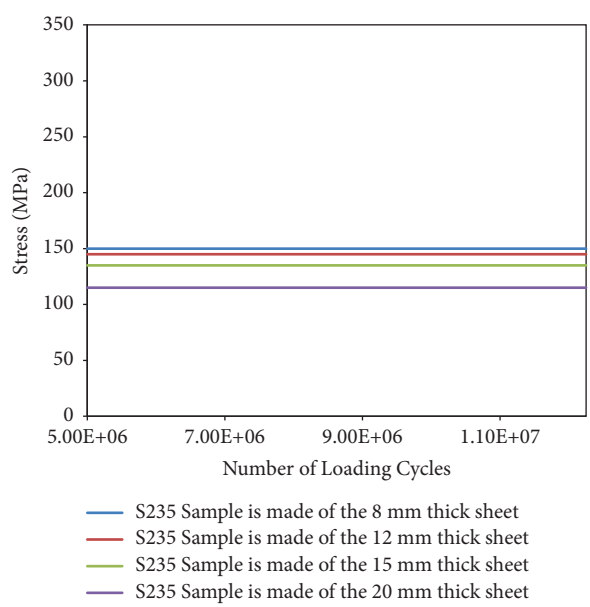

Figure 17: Fitted diagram of the second area of the S-N curve for S235 specimens made of steel plate with thicknesses of 8, 12, 15, and 20 mm.

Table 5: Results of S235 high cycle fatigue test for thicknesses: (a) 8 mm, (b) 12 mm, (c) 15 mm, and (d) 20 mm.

Diameter of specimen	Experimental fatigue limit	Fatigue limit from		The amount of difference with	
		Shigley formula	Weibull formula	Shigley formula	Weibull formula
8	150	150 (reference)	150 (reference)	—	—
12	145	140	147	3%	−1.4%
15	135	137	146	−1.5%	−8%
20	115	133	144	−15%	−20%

Country—W Lost Cany earthquake station in 1994 (see Figure 25) is introduced into the structure and then the history of stress carried out for the bottom of the column is specified in the figure in which the highest amount of stress is applied to this area due to the Northridge earthquake record.

The frame was once modeled with S235 material and again with S355 material. The cross-section of the column for S235

Table 6: Cyclic fatigue test data of S235 steel made of 10 mm thick sheet.

Yield stress: 260 MPa			Ultimate stress: 372 MPa		
Sample number	Sample diameter (mm)	Stress applied (MPa)	The number of cycles	Average number of cycles	Sample status at the end of the cycle
1	5.95		268830		
2	5.92	250	404627	371057	Failure
3	6.01		439715		
4	5.94		595450		
5	5.91	240	630297	628358	Failure
6	5.94		659327		
7	5.95		827124		
8	6.02	230	807659	812358	Failure
9	6.01		802400		
10	5.95		1114521		
11	5.95	220	1120896	1140315	Failure
12	5.95		1185527		
13	5.64		1214591		
14	5.96	210	1228941	1267647	Failure
15	5.96		1359410		
16	6.01		1444297		
17	6.02	200	1450677	1464158	Failure
18	5.94		1497500		
19	5.99		1510297		
20	5.95	190	1551497	1537064	Failure
21	5.96		1549400		
22	5.94		1554200		
23	5.99	180	1775123	1699594	Failure
24	6.01		1769459		
25	6.02		3701311		
26	5.91	170	3549479	3642997	Failure
27	5.96		3678200		
28	5.93		6197897		
29	5.95	160	6596359	6517851	Failure
30	5.98		6759297		
31	5.95		10452400		
32	5.63	150	10387259	10480652	No failure
33	5.98		10602297		
34	5.91		11256759		
35	5.99	145	11452327	11608130	No failure
36	6.01		12115304		

material is as a column with a total depth of 500 and a flange width of 300 and web thickness of 20 and flange thickness of 10 mm, and for a column with S355 material a total depth of 400 and a flange width of 250 and a flange thickness of 20 and a web thickness of 10 mm. The stress history on the column for S235 and S355 materials is depicted in Figure 26.

The number of cycles for different stresses calculated by the rainflow algorithm [3]; this is the most common and most accurate way to count cycles. The rules of rainflow are as follows:

(1) Rearranging the stress-time diagram of the events so that the highest peak or the deepest valley comes first.

(2) Starting from the highest peak (or the lowest valley), go down to the next reversal. The rainflow runs down and continues unless either the magnitude of the following peak (or the following valley, if we started from the lowest valley) is equal to or larger than the peak (or valley) from which it initiated, or a previous rainfiow is encountered.

(3) For the following reversal, follow the same procedure, and so on until the end.

(4) For all ranges and parts of a range that were not used in the previous steps, repeat the procedure.

The result of rainflow is shown in Figure 27. As can be seen from Figure 26, high cyclic fatigue does not matter for the Northridge earthquake record for building with materials S235 and S355 but in the building with corrosion, this record has caused damage to the structure. In fact, in the steel structure with S355 , some lines of the stress, pass through the red area in the figure diagram, which means crossing the fatigue tolerance threshold.

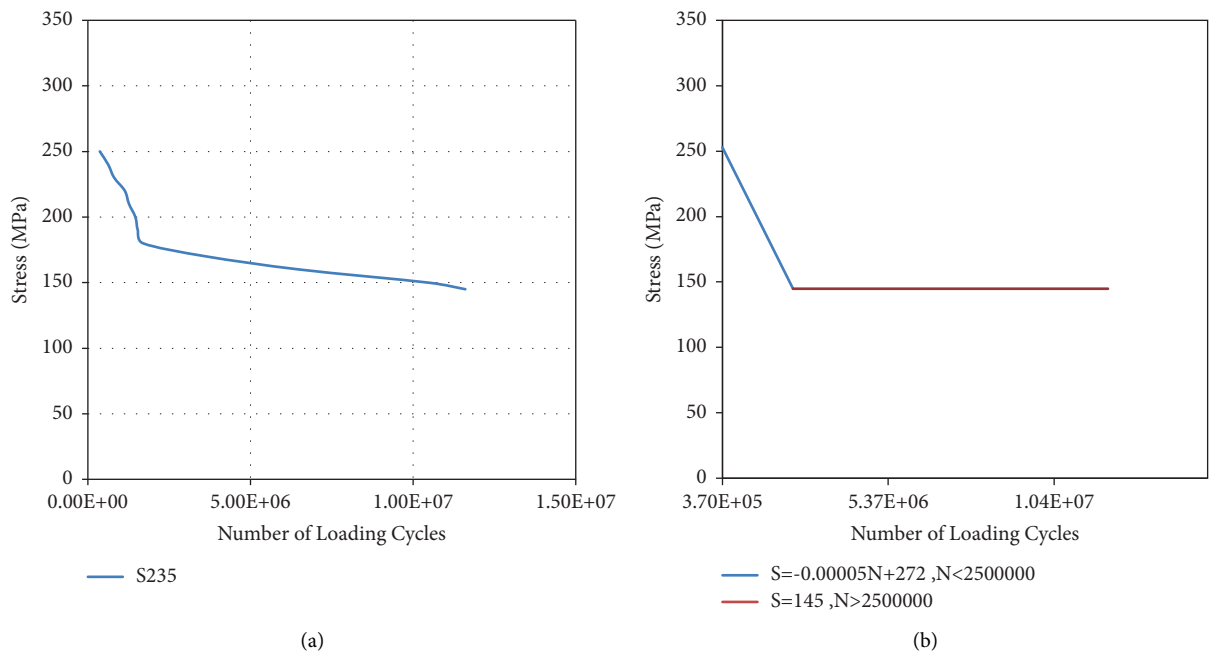

Figure 18: (a) S-N diagram for S235 samples made of steel plate with 10 mm of thickness and (b) fitted diagram of S235.

Table 7: Cyclic fatigue test data of S355 steel made of 10 mm thick sheet.

	Yield stress: 390 MPa			Ultimate stress: 542 MPa	
Sample number	Sample diameter (mm)	Stress applied (MPa)	The number of cycles	Average number of cycles	Sample status at the end of the cycle
1	5.96		50895		
2	5.95	400	50432	50858	Failure
3	5.99		51247		
4	5.65		268396		
5	5.96	395	248659	255831	Failure
6	5.99		250439		
7	6.01		178459		
8	6.03	390	181432	182441	Failure
9	5.92		187432		
10	5.93		375242		
11	5.91	380	367529	361173	Failure
12	5.92		340750		
13	5.64		567476		
14	5.96	370	554375	554080	Failure
15	5.96		540389		
16	5.63		970450		
17	5.95	360	964389	964576	Failure
18	5.96		958888		
19	5.91		1259487		
20	5.95	350	1260348	1265098	Failure
21	5.63		1275459		
22	5.84		1659432		
23	5.98	340	1740400	1715909	Failure
24	5.99		1747896		
25	5.95		2059456		
26	6.01	320	1979869	2013440	Failure
27	6.02		2000997		
28	5.95		2687512		
29	5.94	300	2679436	2654319	Failure
30	5.91		2596010		

Table 7: Continued.

Sample number	Yield stress: 390 MPa Sample diameter (mm)	Stress applied (MPa)	The number of cycles	Ultimate stress: 542 MPa Average number of cycles	Sample status at the end of the cycle
31	5.95		3459658		
32	5.98	260	3654895	3443070	Failure
33	5.99		3214658		
34	5.95		7524136		
35	5.63	250	4500403	5757359	Failure
36	5.98		5247540		
37	5.91		11095900		
38	5.99	245	12694108	11298364	No failure
39	6.01		10105084		
40	5.96		11454300		
41	5.95	240	11564200	11455100	No failure
42	5.99		11346800		
43	5.96		12897989		
44	5.95	200	12984698	12890890	No failure
45	5.98		12789985		

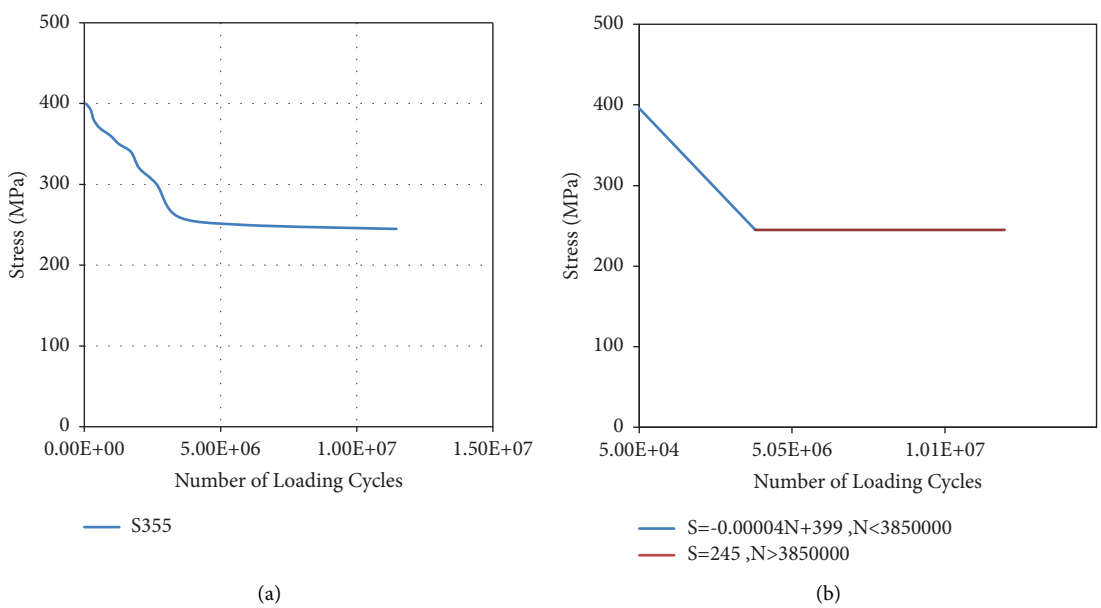

Figure 19: (a) S-N diagram for S355 samples made of steel plate with 10 mm of thickness and (b) fitted diagram of S355.

Table 8: Cyclic fatigue test data of S460 steel made of 10 mm thick sheet.

Sample number	Yield stress: 490 MPa Sample diameter (mm)	Stress applied (MPa)	The number of cycles	Ultimate stress: 680 MPa Average number of cycles	Sample status at the end of the cycle
1	5.97		276792		
2	5.94	383	411349	379134	Failure
3	6.02		449261		
4	5.92		600653		
5	5.93	367	638055	632712	Failure
6	5.91		659427		
7	5.95		835149		
8	6.07	352	810631	817226	Failure
9	6.00		805899		

Table 8: Continued.

Sample number	Yield stress: 490 MPa Sample diameter (mm)	Stress applied (MPa)	The number of cycles	Ultimate stress: 680 MPa Average number of cycles	Sample status at the end of the cycle
10	5.94		1119689		
11	5.96	337	1126928	1146724	Failure
12	5.96		1193553		
13	5.65		1220978		
14	5.96	321	1234737	1272211	Failure
15	5.97		1360915		
16	6.03		1450363		
17	6.02	306	1452423	1468975	Failure
18	5.94		1504139		
19	5.99		1518043		
20	5.97	291	1554605	1540841	Failure
21	5.96		1549875		
22	5.94		1555385		
23	5.99	275	1779446	1702605	Failure
24	6.01		1772982		
25	6.02		3704162		
26	5.91	260	3552156	3646576	Failure
27	5.96		3683407		
28	5.93		6200475		
29	5.95	245	6596926	6519115	Failure
30	5.98		6759943		
31	5.95		10457569		
32	5.65	230	10396714	10486713	No failure
33	5.96		10605856		
34	5.95		11263775		
35	5.99	214	11458578	11613758	No failure
36	5.98		12118919		

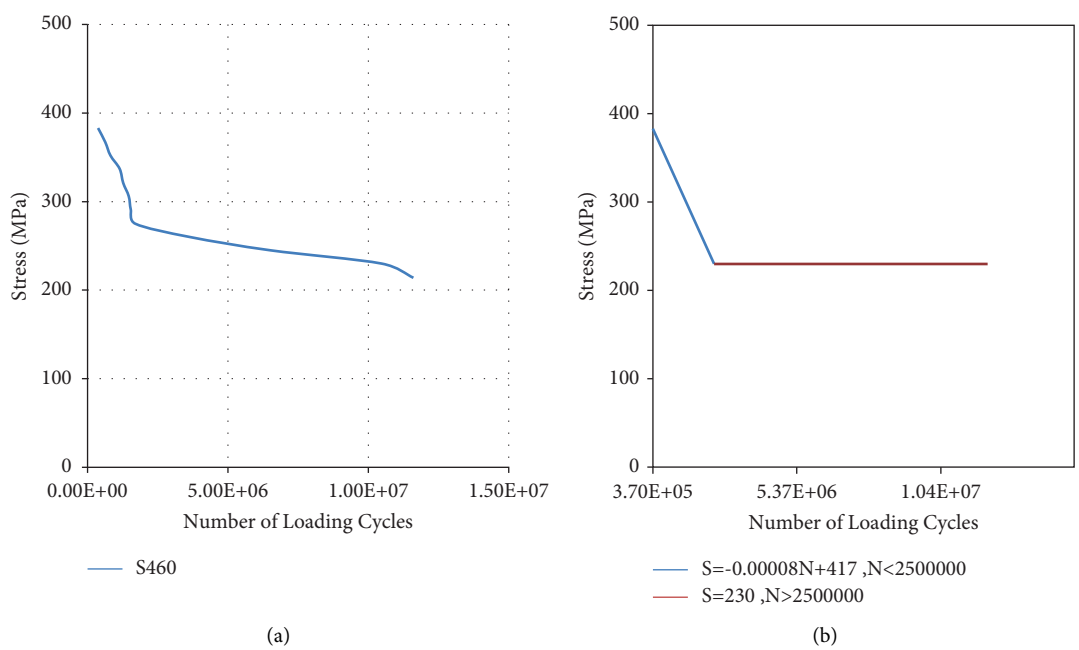

Figure 20: (a) S-N diagram for S460 samples made of steel plate with 10 mm of thickness and (b) fitted diagram of S460.

Table 9: Cyclic fatigue test data of S690 steel made of 10 mm thick sheet.

Yield stress: 656 MPa			Ultimate stress: 780 MPa		
Sample number	Sample diameter (mm)	Stress applied (MPa)	The number of cycles	Average number of cycles	Sample status at the end of the cycle
1	5.97		58570		
2	5.97	600	59072	59003	Failure
3	5.99		59367		
4	5.68		272974		
5	5.94	593	249085	257712	Failure
6	5.96		251077		
7	6.01		186490		
8	6.03	585	187902	189249	Failure
9	5.94		193353		
10	5.95		384915		
11	5.99	570	370881	368670	Failure
12	5.92		350215		
13	5.64		572253		
14	5.94	555	556016	558849	Failure
15	5.96		548277		
16	5.64		979681		
17	5.95	540	970287	972321	Failure
18	5.96		966994		
19	5.91		1261153		
20	5.97	525	1261819	1266379	Failure
21	5.63		1276164		
22	5.84		1666170		
23	5.98	510	1742714	1719041	Failure
24	5.99		1748239		
25	5.97		2066133		
26	6.06	480	1988098	2020979	Failure
27	6.01		2008707		
28	5.95		2690265		
29	5.93	450	2681979	2658772	Failure
30	5.91		2604071		
31	5.96		3461531		
32	5.98	390	3660486	3445689	Failure
33	5.97		3215050		
34	5.95		7524827		
35	5.63	375	4501640	5759884	Failure
36	5.98		5253186		
37	5.91		11101092		
38	5.96	368	12700822	11304225	No failure
39	6.01		10110760		
40	5.96		11460209		
41	5.95	360	11565870	11458223	No failure
42	5.95		11348590		
43	5.95		12903151		
44	5.98	300	12985800	12893846	No failure
45	6.00		12792586		

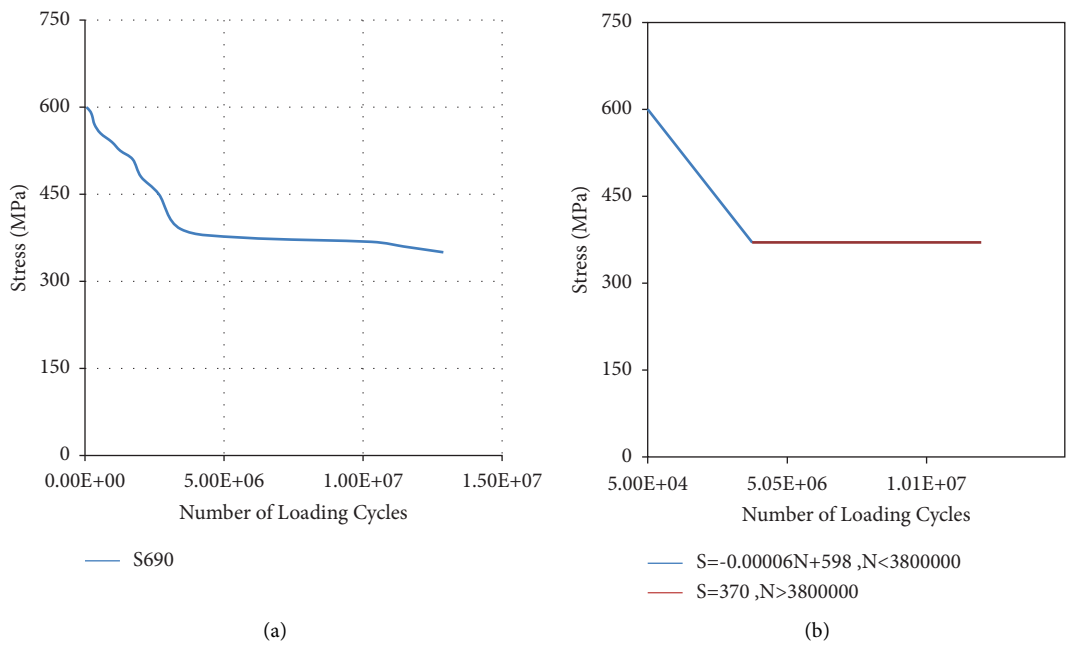

Figure 21: (a) S-N diagram for S690 samples made of steel plate with 10 mm of thickness and (b) fitted diagram of S690.

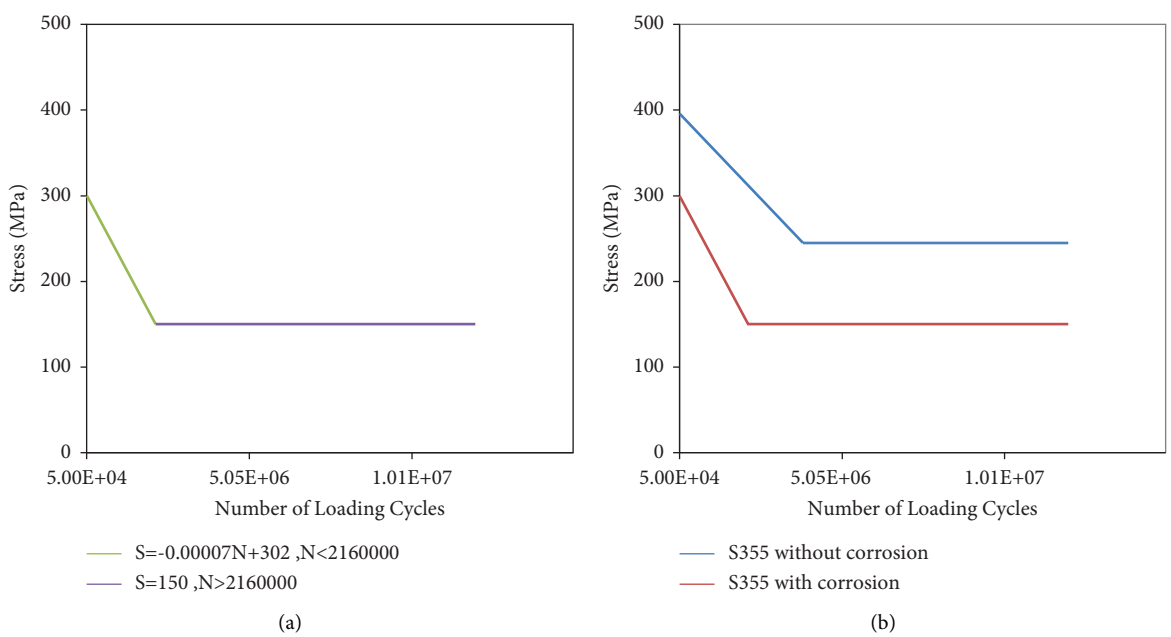

Figure 22: S-N diagram of (a) S355 with corrosion and (b) S355 without corrosion.

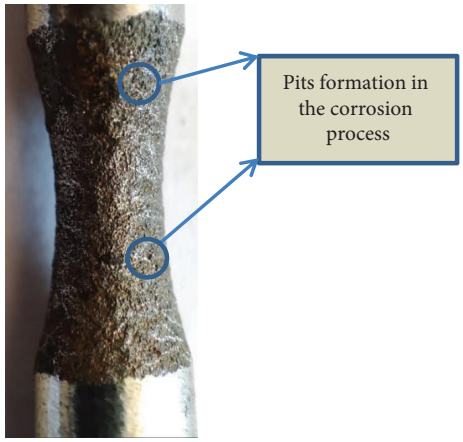

Figure 23: Formation of pits during the uniform corrosion process.

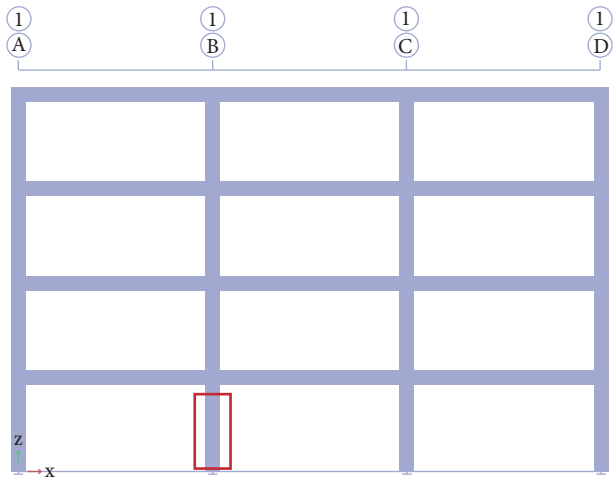

Figure 24: Modeled four-story three span steel moment frames.

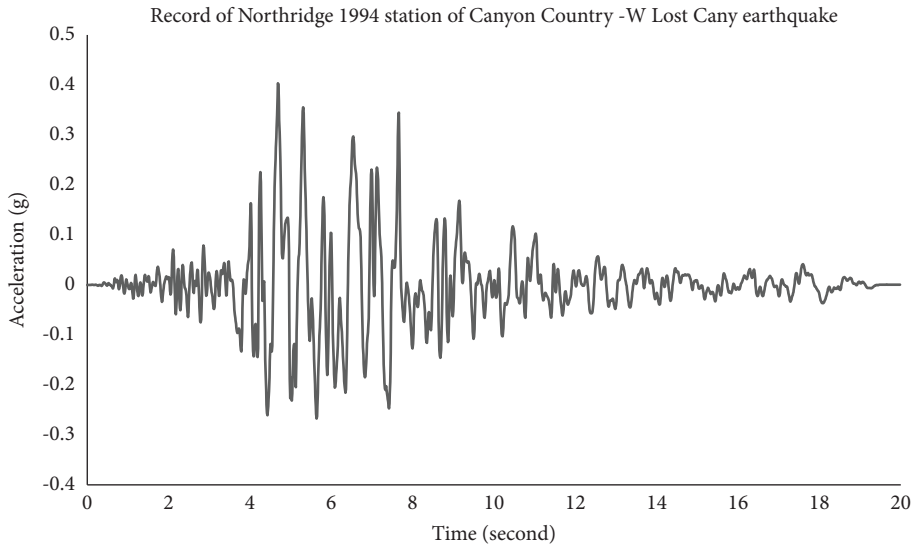

Figure 25: The accelerograph of Northridge earthquake at Canyon Country—W Lost Cany earthquake in 1994.

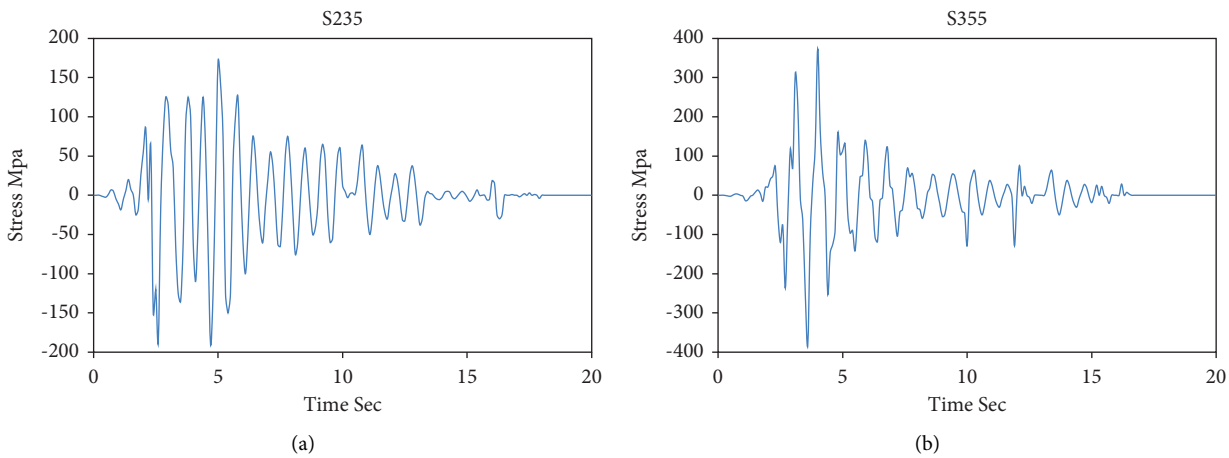

Figure 26: Time history of stress for column with (a) S235 material and (b) S355 material.

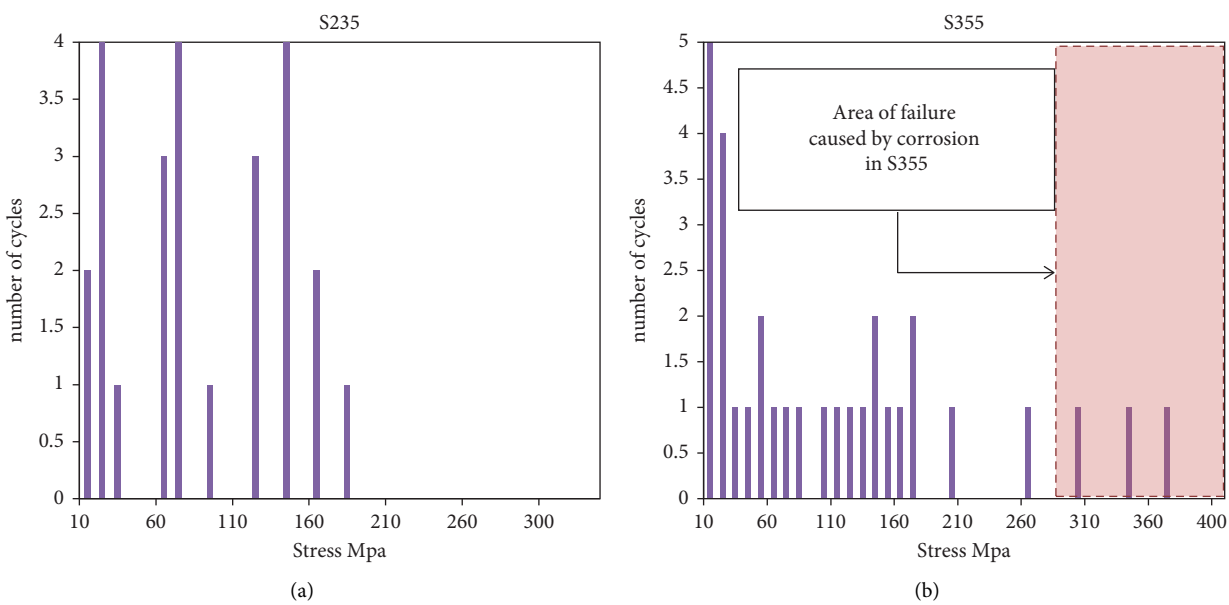

Figure 27: Number of cycles for different stresses for (a) S235 steel and (b) S355 steel.

9. Conclusion

In this study, high cycle fatigue was investigated for S235, S355, S460, and S690 materials. The number of samples used for S460 and S235 was 45 each and S690 and S355 was 36 and for S355 with corrosion was 15. Then, to investigate the effect of the selected plate thickness on cyclic fatigue, four sets of samples, each containing 24 pieces, were made and tested from plates with different thicknesses of 8, 12, 15, and 20 mm. The results of this study for the fatigue limit of the abovementioned materials are as follows:

(i) By changing the thickness of the plates from which the high cycle fatigue samples were made, the fatigue limit was changed about 25%. The reason for this difference is due to the different cooling rates in plates with different thicknesses in the production process and the size effect strongly depends on the average number of defects and inclusions in the material, which increases with thickness.

(ii) The S-N curve has been investigated for two types of high-strength steels, S690 and S460, as well as two types of mild-strength steels, S235 and S355, at 25°C.

(iii) For S355 steel, the ASTM G60-1 standard was used to simulate atmospheric corrosion and by using the ISO 9224 standard, which is an annex to the ISO 9223 standard, the amount of corrosion for 20 years was obtained and the fatigue limit in the case of the sample with corrosion has decreased by 39%.

Then, high cyclic fatigue was calculated for a four-story, three-span frame, once with S235 and again with S355, which inputted the Northridge earthquake record of Canyon Country—W Lost Cany earthquake station in 1994; high cyclic fatigue does not matter for the Northridge earthquake

record for building with materials S235 and S355 without crossing but in the building with corrosion, this record has caused damage to the structure.

Data Availability

The data used to support the study are available from the corresponding author upon request.

Conflicts of Interest

The authors declare that they have no conflicts of interest.

References

[1] J. V. Poncelet, "Introduction à la mécanique industrielle, physique ou expérimentale," *Thiel*, Gallica Limited, Boston, Lincolnshire, 1839.

[2] T. wurde, "Bericht über die Versuche, welche auf der Königl. Niederschlesisch-Märkischen Eisenbahn mit Apparaten zum Messen der Biegung und Verdrehung von Eisen-bahnwagen-Achsen während der Fahrt, angestellt wurden," *Zeitschrift für Bauwesen*, vol. 8, p. 641, 1858.

[3] R. I. Stephens, A. Fatemi, R. R. Stephens, and H. O. Fuchs, *Metal Fatigue in Engineering*, John Wiley & Sons, New York, NY, USA, 2000.

[4] G. Venkataraman, Y.-W. Chung, and T. Mura, "Application of minimum energy formalism in a multiple slip band model for fatigue—II. Crack nucleation and derivation of a generalised Coffin-Manson law," *Acta Metallurgica et Materialia*, vol. 39, no. 11, pp. 2631–2638, 1991.

[5] E. Repetto and M. Ortiz, "A micromechanical model of cyclic deformation and fatigue-crack nucleation in fcc single crystals," *Acta Materialia*, vol. 45, no. 6, pp. 2577–2595, 1997.

[6] D. McDowell, K. Gall, M. Horstemeyer, and J. Fan, "Microstructure-based fatigue modeling of cast A356-T6 alloy," *Engineering Fracture Mechanics*, vol. 70, no. 1, pp. 49–80, 2003.

[7] V. Bennett and D. McDowell, "Polycrystal orientation distribution effects on microslip in high cycle fatigue," *International Journal of Fatigue*, vol. 25, no. 1, pp. 27–39, 2003.

[8] D. McDowell, "Microstructure-sensitive computational fatigue analysis," in *Handbook of Materials Modeling*, pp. 1193–1214, Springer, Berlin, Germany, 2005.

[9] D. L. McDowell, "Simulation-based strategies for microstructure-sensitive fatigue modeling," *Materials Science and Engineering*, vol. 468-470, pp. 4–14, 2007.

[10] A. M. Kanvinde, *Micromechanical Simulation of Earthquake-Induced Fracture in Steel Structures*, Stanford University, Stanford, CA, USA, 2004.

[11] M. Ghaderi, M. Gerami, and R. Vahdani, "Performance assessment of bolted extended end-plate moment connections constructed from grade st-37 steel subjected to fatigue," *Journal of Materials in Civil Engineering*, vol. 32, no. 5, Article ID 04020092, 2020.

[12] M. Ghaderi, M. Gerami, and R. Vahdani, "Experimental assessment and CVGM modeling to investigate the seismic stress– and strain–controlled fatigue properties of st-37 and st-52 Grade steels," *Journal of Materials in Civil Engineering*, vol. 34, no. 4, Article ID 04022005, 2022.

[13] M. Ghaderi, M. Gerami, and R. Vahdani, "Investigating the effect of extremely low cyclic fatigue in steel moment frames with reduced beam section connections," *Journal of Structural and Construction Engineering*, vol. 7, no. 3, pp. 5–19, 2020.

[14] M. Ghaderi, M. Gerami, and R. Vahdani, "A comparison of seismic low cycle fatigue and extremely low cycle fatigue on steel moment frames with reduced beam section connection (RBS)," *International Journal of Fatigue*, vol. 119, pp. 139–149, 2019.

[15] G. B. Richard, *shigley's mechanical engineering design*, McGraw-Hill Education, New York, NY, USA, 2019.

[16] N. Perez, *Linear Elastic Fracture Mechanics*, Springer, Berlin, Germany, 2004.

[17] M. Pietrzyk, L. Cser, and J. Lenard, *Mathematical and Physical Simulation of the Properties of Hot Rolled Products*, Elsevier, Amsterdam, The Netherlands, 1999.

[18] R. M. Pidaparti and A. S. Rao, "Analysis of pits induced stresses due to metal corrosion," *Corrosion Science*, vol. 50, no. 7, pp. 1932–1938, 2008.

[19] M. M. Kashani, A. J. Crewe, and N. A. Alexander, "Use of a 3D optical measurement technique for stochastic corrosion pattern analysis of reinforcing bars subjected to accelerated corrosion," *Corrosion Science*, vol. 73, pp. 208–221, 2013/08/01/2013.

[20] Y. Wang, S. Xu, H. Wang, and A. Li, "Predicting the residual strength and deformability of corroded steel plate based on the corrosion morphology," *Construction and Building Materials*, vol. 152, pp. 777–793, 2017.

[21] S. Xu, Z. Zhang, and G. Qin, "Study on the seismic performance of corroded H-shaped steel columns," *Engineering Structures*, vol. 191, pp. 39–61, 2019.

[22] G. A. MacRae and K. Kawashima, "Seismic behavior of hollow stiffened steel bridge columns," *Journal of Bridge Engineering*, vol. 6, no. 2, pp. 110–119, 2001.

[23] J. C. Anderson and R. G. Johnston, "Performance of steel frame building which experienced intense ground motion," *Journal of Performance of Constructed Facilities*, vol. 12, no. 4, pp. 186–198, 1998.

[24] P. P. Milella, *Fatigue and Corrosion in Metals*, Springer Science & Business Media, Berlin, Germany, 2012.

[25] International Organization for Standardization Iso 1143, *Metallic Materials–Rotating Bar Bending Fatigue Testing*, I. O. f. Standardization, Geneva, Switzerland, 2010.

[26] M. G. Fontana, *Corrosion Engineering*, McGraw-Hill, Singapore, 1987.

[27] Iso 9223:2012, I. Standard, "Corrosion of metals and alloys Corrosivity of atmospheres Classification, determination and estimation," 2012, https://www.iso.org/standard/53499.html.

[28] Iso 9224, I. Standard, "Corrosion of metals and alloys—corrosivity of atmospheres—guiding values for the corrosivity categories," 2012, https://cdn.standards.iteh.ai/samples/53500/48d0ad5886f74a05a0d0faf4a71da09e/ISO-9224-2012.pdf.

[29] Astm G60-01(2018), "A. International, standard practice for conducting cyclic humidity exposures," 2018, https://www.astm.org/.

[30] En 1993-5, E. Standard, "The European union edict of government," 2007, https://www.phd.eng.br/wp-content/uploads/2015/12/en.1993.5.2007.pdf.

[31] J. Shigley and L. Mitchell, *Mechanical Engineering Design*, McGraw-Hill Book Company, New York, NY, USA, 1983.

[32] Y. Li, R. Song, and J. W. Van De Lindt, "Collapse fragility of steel structures subjected to earthquake mainshock-aftershock sequences," *Journal of Structural Engineering*, vol. 140, no. 12, Article ID 04014095, 2014.